# Predicting the failure of ultrathin porous membranes via bulge test

Steven R. Gillmer[a], Niaz Abdolrahim[a,b], Sarah E. Wayson[c], Joshua D. Winans[c], David Z. Fang[d,†], Jon-Paul S. DesOrmeaux[e], Jirachai Getpreecharsawas[c,f], Jonathan D. Ellis[a,g], Philippe M. Fauchet[d,‡], James L. McGrath[c,*]

[a]Department of Mechanical Engineering, University of Rochester; Rochester, NY, USA

[b]Materials Science Program, University of Rochester; Rochester, NY, USA

[c]Department of Biomedical Engineering, University of Rochester; Rochester, NY, USA

[d]Department of Electrical and Computer Engineering, University of Rochester; Rochester, NY, USA

[e]SiMPore Inc., West Henrietta, NY, USA

[f]Microsystems Engineering, Rochester Institute of Technology, Rochester, NY, USA

[g]The Institute of Optics, University of Rochester; Rochester, NY, USA

[†]Current address : Booz Allen Hamilton Inc., Arlington, VA, USA

[‡]Current address : Department of Electrical Engineering and Computer Science, Vanderbilt University, Nashville, TN, USA

[*]Corresponding author. Tel. + 1(585)273-5489; *e-mail address:* jmcgrath@bme.rochester.edu

**Abstract**

Silicon nanomembranes are ultrathin nanoporous materials with extraordinary permeability and a variety of applications ranging from DNA sequencing to compact hemodialysis. Although the deflections and stresses of the nanomembranes can be reliably predicted, a straightforward and tenable failure mechanism has yet to be outlined. In this publication, a new brittle macroscale failure model is established and validated with experimental results. Theoretical agreement with experiments within 10% accuracy offers reliable failure predictions for square membrane dimensions from 60 μm to 1.5 mm. Furthermore, our experiments elucidate fracture toughness values of nanomembranes made of amorphous silicon and non-stoichiometric silicon nitride. We conclude that the nanomembranes fail under a combination of bending and tensile stress along the edge of the membranes and our observed fracture toughness values are in good agreement with previously published work. The predictive model will be useful in the selection of nanomembranes for particular applications and will help guide the design of new materials with improved strength. The model should also prove useful for high-volume, in-line processing and inspection of nanomembranes as their role becomes more prominent in industry.

# 1 Introduction

The increased ductility of nanocrystalline ceramics at room temperature [1] has enabled a variety of promising technologies. Specifically, ultrathin nanocrystalline membranes have the ability to withstand relatively high differential pressures without undergoing permanent mechanical yield [2]. Porous nanocrystalline silicon (pnc-Si) and porous $SiN_x$ (nanoporous nitride or NPN) membranes have leveraged their strength to demonstrate size-selective protein separations [3], new avenues for cell culture and tissue engineering [4, 5], a novel form of low-voltage electroosmosis [6], a novel form of chemical capacitive sensing [7], high resolution DNA sequencing [8], and a potential replacement for current hemodialysis devices with increased performance and compact size [9–11]. As the development of these technologies currently stands, the fabrication and control of pore properties is understood and documented [9, 12, 13], stresses and deflections of the membranes are predictable [14–16]; however, a straightforward and conclusive failure mechanism has yet to be realized.

The most promising failure criteria has been published by Kovács, *et al.* [17, 18]. Their work accurately predicts the failure of ceramic membranes with micrometer-size pores with the incorporation of finite element analysis (FEA) and a required calibration factor to match experiments. Although the theory is reliable, it assumes the failure of the membranes occurs when the maximum principle stress in the material is attained. Indeed, this brittle failure mechanism can be considered valid; however, the work of Merle and Göken [2] suggests the use of Griffith's law [19] as a notably reliable approach to analyze the fracture of amorphous non-porous $Si_3N_4$ membranes without the need for FEA.

In this publication, we assimilate the tenable findings from Kovács, *et al.* as well as Merle and Göken and build on their conclusions to predict the failure of ultrathin and porous silcon-based membranes. An imperative finding of the finite element simulations performed by Kovács, *et al.* is that thin membranes produce maximum stess concentrations at the middle of the edges due to a large bending moment. Merle and Göken negate that bending concentration since their fabricated defects were in the center of the membrane; thereby promoting failure at that point. Our membranes are porous over the entire area, and as a result, the bending moment at the edge plays a critical role in the overall failure mechanism.

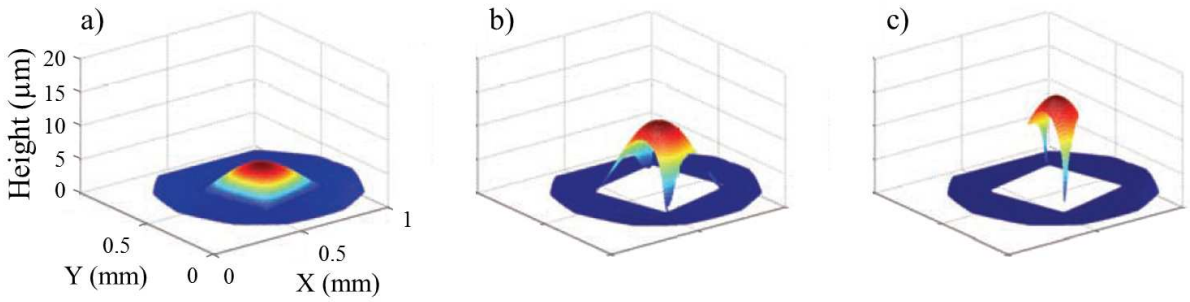


Figure 1: White light interferometric measurement (via Veeco Wyko NT1100 Optical Profiling System) of the deformation of a 400 μm × 400 μm square pnc-Si membrane under 0.69, 2.07, and 3.45 kPa (0.1, 0.3, and 0.5 psi) of pressure using the setup shown in Figure 4. Bending stress concentrations at the edge of the membrane eventually catalyze failure of the structures. High slopes at the edges of the membrane are not apparent in (b) and (c) due to unresolvable fringe densities in the interferometer.

White light interferometric measurements of a 400 μm × 400 μm square pnc-Si membrane under applied pressure are shown in Figure 1 to illustrate the amount of bending that occurs towards the edges of the membranes. Figure 2a shows a SEM image of a square membrane after failure. The fact that the membrane failed at all edges simultaneously is also consistent with the role of bending stresses at membrane edges causing failure. Finally, as evidence of the brittle nature of the nanomembranes, Figure 2b shows the fracture of a rectangular membrane with a very high aspect ratio (100 μm × 6 mm). In this geometry, fracture begins along the narrow ends and propagates down the long axis. The observed propagating crack illustrates the brittle nature of the material.

To predict these effects, we have developed a macroscopic model that can reliably produce the brittle failure of porous silicon-based nanomembranes and have validated it with experimental results. The theory combines the principles of Timoshenko [14] with the appropriate weighting [16] to accurately predict stresses within the material under a bulge test scenario [15]. Under this criteria the pores in the material act as defects which can be related to failure using Griffith's Law [19]. To match experiments, fracture toughness is left as a free parameter.

In comparison to the work by Kovács, *et al.*, our approach does not require FEA for accuracy and can be used in a straightforward fashion. Compared to Merle and Göken, we observe lower fracture toughness values of our porous membranes compared to their non-porous counterparts. Merle and Göken examined pure tensile failure of amorphous $Si_3N_4$ nanomembranes while our experiments create a combination of bending and tensile stress-induced failure. To reinforce our results, our

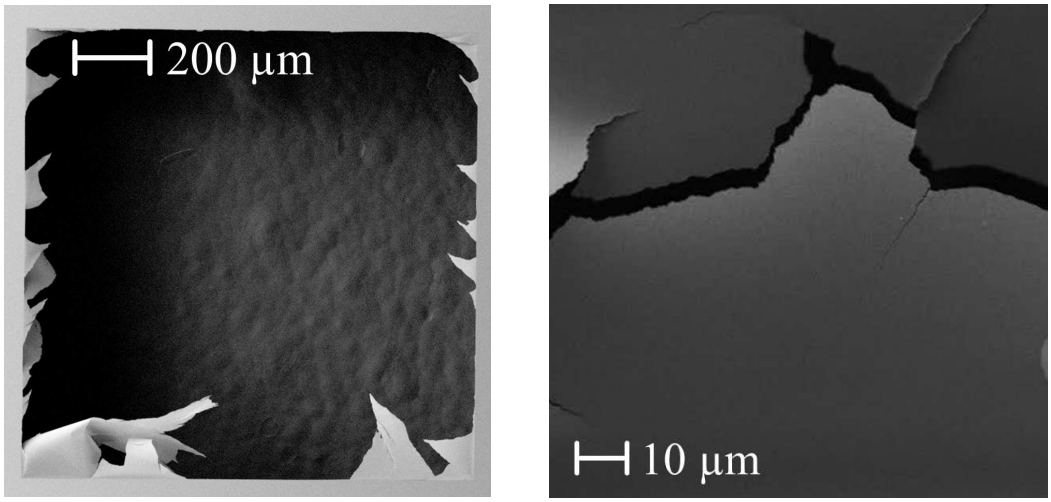


(a) (b)

Figure 2: Scanning electron microscope images demonstrating the brittle failure of the porous membranes. (a) Stress concentrations from large bending moments at the edges of the square membranes produce sudden and catastrophic failure. (b) Propagating cracks are easily observed in a rectangular membrane (100 µm × 6 mm) to appreciate the brittle nature of the material.

observed fracture toughness values are in good agreement with those observed by Matoy, *et al.* for similar silicon-based materials subjected to bending stresses that promote fracture [20].

## 2 Construction of membranes

Varying construction processes can yield different structural properties of the membranes as previously mentioned by Merle and Göken [2] as well as Kovács [18]. Methods for fabrication and control of pore properties in pnc-Si and NPN membranes have been published with extensive detail [9,13]. In this section, we briefly outline fabrication methods for completeness and accessible comparisons to our work. Figure 3 provides the process flow used to construct both types of nanoporous membranes used for this research.

**Porous nanocrystalline silicon (pnc-Si)**

The approach to fabricate pnc-Si membranes utilizes silicon deposition techniques combined with etching processes. Directly patterning the pores is exceedingly time consuming and not fit to

achieve industrial-scale throughput. Instead, the pores are spontaneously formed during a rapid thermal anneal whereby nanocrystals nucleate from amorphous silicon.

The first step in the process involves growing a ∼500 nm-thick layer of $SiO_2$ on both sides of a silicon substrate. The back side of the wafer is then patterned using photolithography to form an etch mask and the front oxide layer is removed and replaced with a three layer stack using RF magnetron sputtering. The pnc-Si membranes used in this research are 20 nm thick; thus, the stack is composed of 20 nm $SiO_2$/ 20 nm amorphous Si/ 20 nm $SiO_2$. This deposition recipe is well characterized, and can deposit films with ±1% thickness accuracy and surface roughnesses under 0.5 nm [9].

To form the pores in pnc-Si, the wafer is briefly exposed to a high temperature (715-770°C for 30 s) in a rapid thermal processing chamber. The backside of the wafer is then etched using EDP (ethylenediamine pyrocatechol) which removes material along the (111) plane of the Si substrate. As a final step, the wafer is exposed to a buffered oxide etchant to remove oxide layers – thereby exposing the freestanding pnc-Si membrane. The membranes then tend to grow a native oxide layer that stabilizes at approximately ∼1.5 nm over the course of one week after being exposed to ambient air.

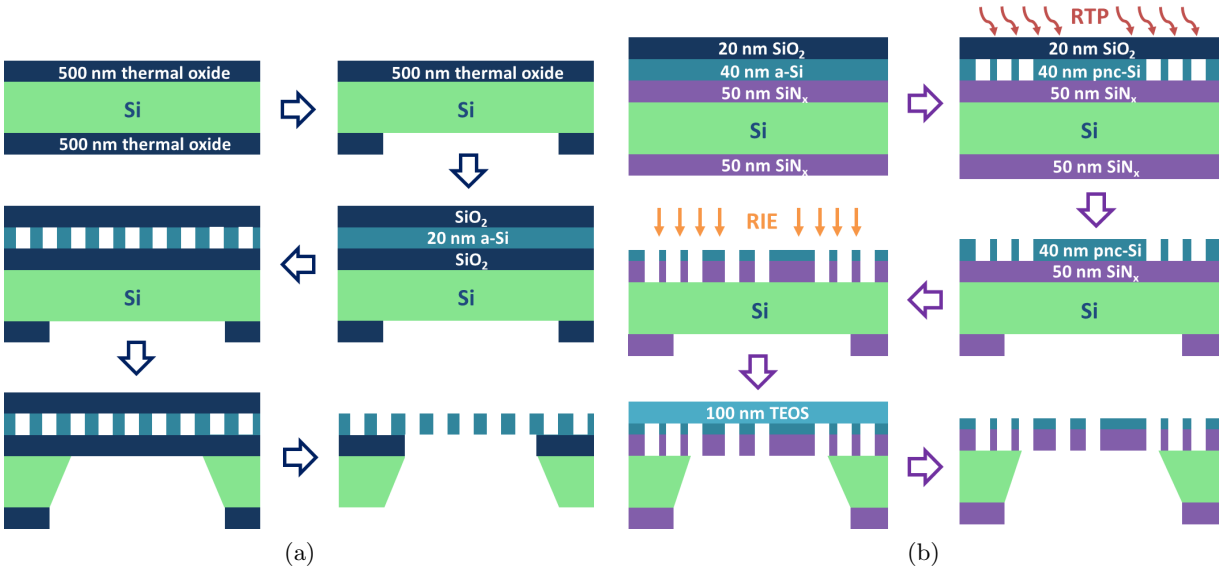


Figure 3: Process flows for construction of porous membranes made of (a) porous nanocrystalline silicon (pnc-Si) and (b) nanoporous nitride (NPN). Step-by-step processes are outlined in the text.

**Nanoporous nitride (NPN)**

The process used to create freestanding pnc-Si membranes is adapted for use as a mask in the fabrication of NPN [13]. The first step involves forming a 40 nm pnc-Si layer using a 50 nm $SiN_x$/ 40 nm amorphous Si/ 20 nm $SiO_2$ stack on the front side of the wafer. The backside is also coated with $SiN_x$. The thickness of the amorphous silicon layer is maximized to enable a longer etch through the $SiN_x$ after pores form in pnc-Si. To create pores, the wafer is exposed to a rapid thermal process (RTP in Figure 3) as outlined previously.

The backside $SiN_x$ layer is patterned to create an etch mask and the frontside is exposed to a reactive ion etching (RIE) process which transfers the pnc-Si pores to the $SiN_x$ layer. Next, using tetraethyl orthosilicate (TEOS) as a precursor gas, a 100 nm $SiO_2$ layer is deposited on the front surface using plasma-enhanced chemical vapor deposition (PECVD). The $SiO_2$ layer protects the NPN during the bulk silicon etch from the backside of the wafer. The final step removes the protective $SiO_2$ layer to expose the freestanding NPN membrane.

A variety of pnc-Si and NPN nanomembranes were constructed from both materials in square geometries ranging from 0.06 mm to 1.75 mm on a side. They were then subjected to a bulge test [15] until failure occurred [13]. Our objective was to develop a predictive theory that anticipated the pressures at which the nanomembranes failed.

# 3 Failure Mechanism

In 1921, Alan Griffith published a seminal paper [19] relating the strength of brittle materials to the sizes of their inherent defects and flaws rather than the intrinsic strength of their atomic bonds. Since then a general description of his findings, known as Griffith's Law, has become a cornerstone of fracture mechanics:

$$K_{Ic} = \sigma_{total} Y \sqrt{\pi a}. \tag{3.1}$$

Equation 3.1 relates the fracture toughness of a material, $K_{Ic}$, to the internal stress , $\sigma_{total}$ (in our case a combination of bending, tension and residual), a dimensionless crack geometry and location factor, $Y$, and half the width of the defect or crack, $a$. Our hypothesis in this work is

that the introduction of pores into a ultrathin membrane geometry drives failure of the membranes because the pores act as defects. Griffith's law was originally proposed for bulk materials; however, our experiments demonstrate the theory applies to thin nanomembranes as well. The reliable application of this theory to thin membranes reinforces the work of Merle and Göken [2].

The majority of the following discussion is focused on realizing a critical stress, $\sigma_{total}$, within the material to use in Griffith's Law. To determine internal stress throughout a membrane during a bulge test, van Rijn, *et al.* [16] have proposed the weighted superposition of two-dimensional deflection and stress equations with the three-dimensional deflections and stresses derived by Timoshenko [14]. We further expand their theory to include the residual stress of our nanomembranes which plays a role in ultimate fracture toughness values.

Following the example of Van Rijn, we first consider a two-dimensional clamped membrane subjected to a uniform pressure, $q$. A diagram of one such membrane in a bulge test experimental setup is shown in Figure 4 and has length, $l$, thickness, $h$, and is subjected to a tensile force, $S$, as the membrane deforms under an applied load. The deflection of the membrane, $w$, is a function of its horizontal position, $x$, and assumes clamped boundary conditions.

Van Rijn, *et al.* derive a constant tensile stress in this two-dimensional material as [16]

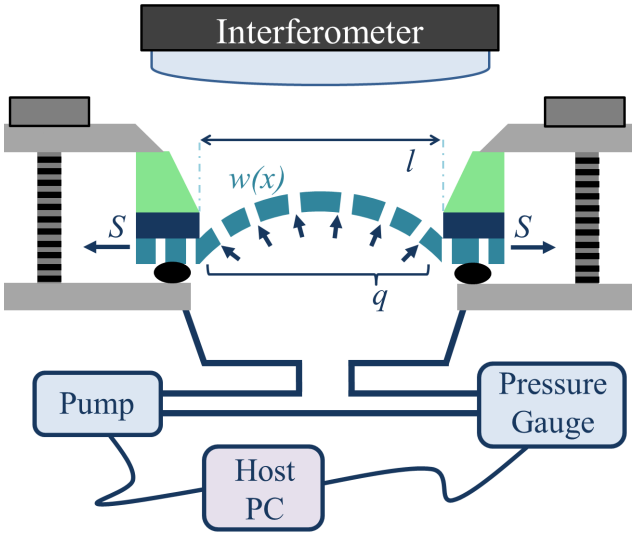


Figure 4: The initial two-dimensional case used to derive intrinsic stress in a bulge test scenario [15]. A membrane clamped at two edges is subjected to a uniform pressure, $q$. The membrane has length, $l$, thickness, $h$, and is subjected to a tensile force, $S$ as the membrane deforms under an applied load. The deflection of the membrane, $w$ is a function of its horizontal position, $x$.

$$\sigma_t = \frac{S}{h} = \frac{Eu^2}{3(1-\nu^2)}\Big(\frac{h}{l}\Big)^2, \tag{3.2}$$

where $E$ is Young's Modulus and $\nu$ is Poisson's ratio. Equation 3.2 is a function of the dimensionless parameter, $u$, that is defined by

$$u^6 = \frac{9(1-\nu^2)^2 q^2 l^8}{8E^2 h^8}. \tag{3.3}$$

Equation 3.3 holds true for the case that $u \gg 1$ which is generally satisfied for large deflections in membranes which are much thinner then they are wide. Furthermore, the bending stress at the edge of the membrane plays a critical role in the overall stress distribution:

$$\sigma_b = \frac{3q}{2u\tanh(u)}\Big(\frac{l}{h}\Big)^2. \tag{3.4}$$

Under the condition $u \gg 1$ the term $\tanh(u)$ approaches unity, and thus Equation 3.4 becomes

$$\sigma_{b,u\gg 1} = \frac{3q}{2u}\Big(\frac{l}{h}\Big)^2. \tag{3.5}$$

The reader is referred to Ref. [16] for further derivations of the above terms.

Timoshenko [14] has used the principles of virtual displacements to calculate the tensile stress at the middle of a square membrane clamped at all four edges as

$$\sigma_m = \frac{E}{1-\nu} 1.848 \frac{\omega_0^2}{l^2}, \tag{3.6}$$

where the central deflection, $\omega_0$, is given by

$$\omega_0 = 0.318 l \Big(\frac{ql}{Eh}\Big)^{(1/3)}. \tag{3.7}$$

Under the assumption that failure will occur near the middle of the clamped edges, van Rijn, *et al.* suggest the following weighted superposition between the two-dimensional and three-dimensional case:

$$\sigma_{combined} = \sigma_m\big(1 + \frac{\sigma_b}{\sigma_t}\big). \tag{3.8}$$

Their assumption is also dependent on the ratio between $\sigma_b$ and $\sigma_t$ scaling identically at the edge of the membrane so that the ratio between them remains constant. Finally, we incorporate the residual stress in our membranes with a simple addition:

$$\sigma_{total} = \sigma_{combined} + \sigma_r. \tag{3.9}$$

Equation 3.9 is combined with Equation 3.1 to produce a complete failure criteria for the membranes. The resulting equation is rearranged to form

$$q_f = \sqrt{\Big(\frac{K_{Ic}}{Y\sqrt{\pi a}C_\nu} - \frac{\sigma_r}{C_\nu}\Big)^3 \frac{h^2}{l^2 E}}, \tag{3.10}$$

where $C_\nu$ is a constant derived from Equations 3.2, 3.5 and 3.6 that depends on Poisson's ratio. For our membranes made out of NPN ($\nu = 0.28$ from Ref. [15]) and pnc-Si ($\nu = 0.22$ from Ref. [21]) Equations 3.2, 3.5 and 3.6 reduce to

$$\sigma_{t,\mathrm{NPN}} = 0.356\sqrt[3]{\frac{q^2 l^2 E}{h^2}}; \quad \sigma_{b,u\gg1,\mathrm{NPN}} = 1.511\sqrt[3]{\frac{q^2 l^2 E}{h^2}}; \quad \sigma_{m,\mathrm{NPN}} = 0.260\sqrt[3]{\frac{q^2 l^2 E}{h^2}} \tag{3.11}$$

$$\sigma_{t,\mathrm{pnc-Si}} = 0.352\sqrt[3]{\frac{q^2 l^2 E}{h^2}}; \quad \sigma_{b,u\gg1,\mathrm{pnc-Si}} = 1.495\sqrt[3]{\frac{q^2 l^2 E}{h^2}}; \quad \sigma_{m,\mathrm{pnc-Si}} = 0.240\sqrt[3]{\frac{q^2 l^2 E}{h^2}}. \tag{3.12}$$

Thus the above expressions can be rearranged in the form of Equation 3.10 to predict the pressures, $q_{f,\mathrm{NPN}}$ and $q_{f,\mathrm{pnc-Si}}$ at which the membranes will fail:

$$q_{f,\mathrm{NPN}} = \sqrt{\Big(\frac{K_{Ic}}{Y\sqrt{\pi a}(1.364)} - \frac{\sigma_r}{1.364}\Big)^3 \frac{h^2}{l^2 E}} \tag{3.13}$$

$$q_{f,\mathrm{pnc-Si}} = \sqrt{\Big(\frac{K_{Ic}}{Y\sqrt{\pi a}(1.259)} - \frac{\sigma_r}{1.259}\Big)^3 \frac{h^2}{l^2 E}}. \tag{3.14}$$

We define $Y \approx 1.1$ which designates that failure will occur near the edge of the clamped membrane [22] where stress concentrations are highest.

Young's moduli and residual stresses of the porous membranes were directly measured using the bulge test technique [15]. The method requires a data fit using a least-squares regression algorithm with Young's modulus and residual stress as parameters under the formalism

$$q = C_1 \sigma_r h \frac{w_c}{(l/2)^2} + C_2 M h \frac{w_c^3}{(l/2)^4}. \tag{3.15}$$

The $C_1$ and $C_2$ coefficients are dependent on the membrane geometry and the film's Poisson ratio, $\nu$, $q$ is the pressure applied to the membrane, $\sigma_r$ is the films residual stress, $h$ is the thickness of the film, $w_c$ is the vertical displacement at the center of the membrane, $l$ is the length of the square window, and $M$ is the biaxial modulus, $E/(1-\nu)$, for an isotropic film. For a square membrane, Vlassak calculated $C_1 = 3.393$ and $C_2 = (0.792 + 0.085\nu)^{-3}$ using energy minimization techniques to match the free energy of the membrane with the membrane displacement field [15].

Porosity typically affects the Young's moduli and residual stresses of the materials. To incorporate the effect, solid Young's modulus can be scaled as $E_p = (1-P)E_s$ where $P$ is the membrane porosity, $E_p$ is porous Young's modulus, and $E_s$ is the solid Young's modulus [17, 23]. Likewise, residual stress can be scaled according to $\sigma_{r,p} = (1-P)\sigma_{r,s}$. A notable departure from this model was observed by Kovács, *et al.* [18] which required additional exponential scaling of the porosity. In this work, we avoid all porosity scaling ambiguities by measuring the porous Young's moduli and residual stresses *in situ* via Equation 3.15; therefore, no scaling is required. Bulge test results are shown in Figure 5. The porous pnc-Si membrane in Figure 5 had a sidewall length of 67 µm and the NPN membranes had sidewall lengths of 278 µm. An exploration of the model sensitivity in the following section will demonstrate that it is absolutely critical to accurately measure sidewall lengths for small membrane geometries such as these. For reliable bulge test results on larger membranes, the requirement is not as stringent.

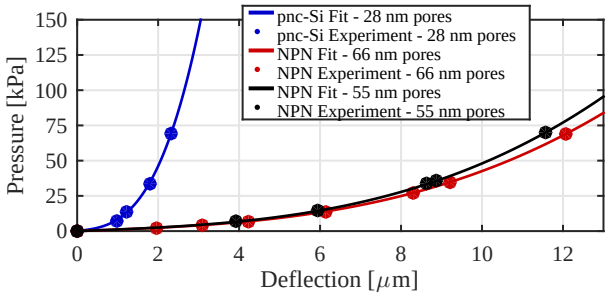


Figure 5: Experimental data obtained using the bulge test to measure Young's moduli and residual stresses of the porous membranes *in situ*. Measured parameters are outlined in Table 1. (Color online)

# 4 Experimental Results

To determine membrane burst pressures, bulge test experiments were conducted with increasing pressure until membrane failure. In these experiments, the front side of the membrane was always facing the applied pressure as shown in Figure 4. This orientation ensures delamination effects did not play a role in failure. Equations 3.13 and 3.14 were then incorporated into MATLAB to compare theory against experiment. Results are shown in Figure 6 and a set of parameters, including best fit estimates of $K_{Ic}$, are found in Table 1. The error bars on Figure 6 represent $\pm$ one standard deviation. Standard deviations of the pnc-Si failure pressures are based on a minimum of 19 trials and standard deviations of all NPN failure results are based on a minimum of four trials. The agreement between experiment and theory in Figure 6 proves Griffith's Law is reliable for high-volume, in-line prediction of failure based on nominal parameters.

For 50 nm thick NPN films with 66 nm pores and 20% porosity, $K_{Ic} \approx 1.45$ MPa$\sqrt{\text{m}}$; for 50 nm thick NPN films with 55 nm pores and 14% porosity, $K_{Ic} \approx 1.41$ MPa$\sqrt{\text{m}}$; and for 20 nm thick pnc-Si films with 28 nm pores and 7% porosity, $K_{Ic} \approx 0.98$ MPa$\sqrt{\text{m}}$. Using these values for $K_{Ic}$, our model can predict mean membrane failure pressures within 10% accuracy for square membrane dimensions from 60 μm to 1.5 mm.

Exploring the parameter space of the simulation offers insight into the sensitivity of the model and may identify design strategies for creating stronger membranes. Figure 7 shows predicted changes in the burst pressures of pnc-Si membranes as a function of fracture toughness, porosity, residual stress, pore size, membrane thickness, and error in side length measurement. The exploration shows the most significant changes in burst pressure occur with variations in fracture

Table 1: Material properties used to validate the macroscale model.

| Material | Pore Size (nm) | Thickness (nm) | Fracture Toughness (MPa$\sqrt{\text{m}}$) | Porous Young's Modulus (GPa) | Residual Stress (MPa) | Poisson's Ratio | Porosity |
|---|---|---|---|---|---|---|---|
| pnc-Si | 28 | 20 | 0.98 | 128 | 57 | 0.22 | 7% |
| NPN | 66 | 50 | 1.45 | 93 | 122 | 0.28 | 20% |
| NPN | 55 | 50 | 1.41 | 108 | 127 | 0.28 | 14% |

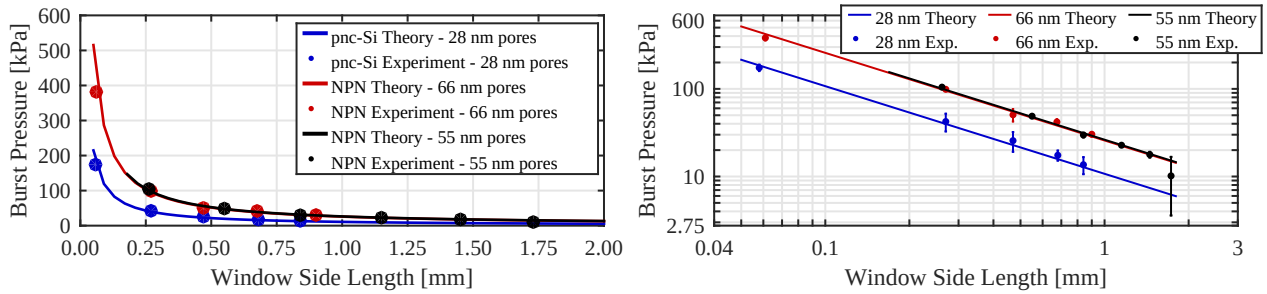


(a) (b)

Figure 6: Predicted burst pressures vs. measurement for square membranes on (a) a linear scale and (b) a log-log scale. Error bars represent ± one standard deviation of experimental results. (Color online)

toughness (a), pore size (d), and membrane thickness (e), while changes in porosity (b) and residual stress (c) have minimal effects on the failure of the material. Inaccuracy in the measured side lengths of square membranes (f) are shown to have a much more significant effect on smaller membranes compared to larger ones. The main conclusion to be drawn from Figure 7f is that a slight error in the measurement of window lengths (*e.g.* $\approx 10\mu$m) could easily be the dominant source of error in burst pressure measurements.

A final remark should be made in regards to the deduction that higher porosities yield slightly higher strengths of the material (Figure 7b). Although mathematical porosity scalings were not required for the values in Table 1, the simulation in Figure 7b assumes the relationships $E_p = (1-P)E_s$ and $\sigma_{r,p} = (1-P)\sigma_{r,s}$ which decrease the effective Young's moduli and residual stresses with higher porosities. These scalings generally make the membrane more flexible and therefore more resistant to failure.

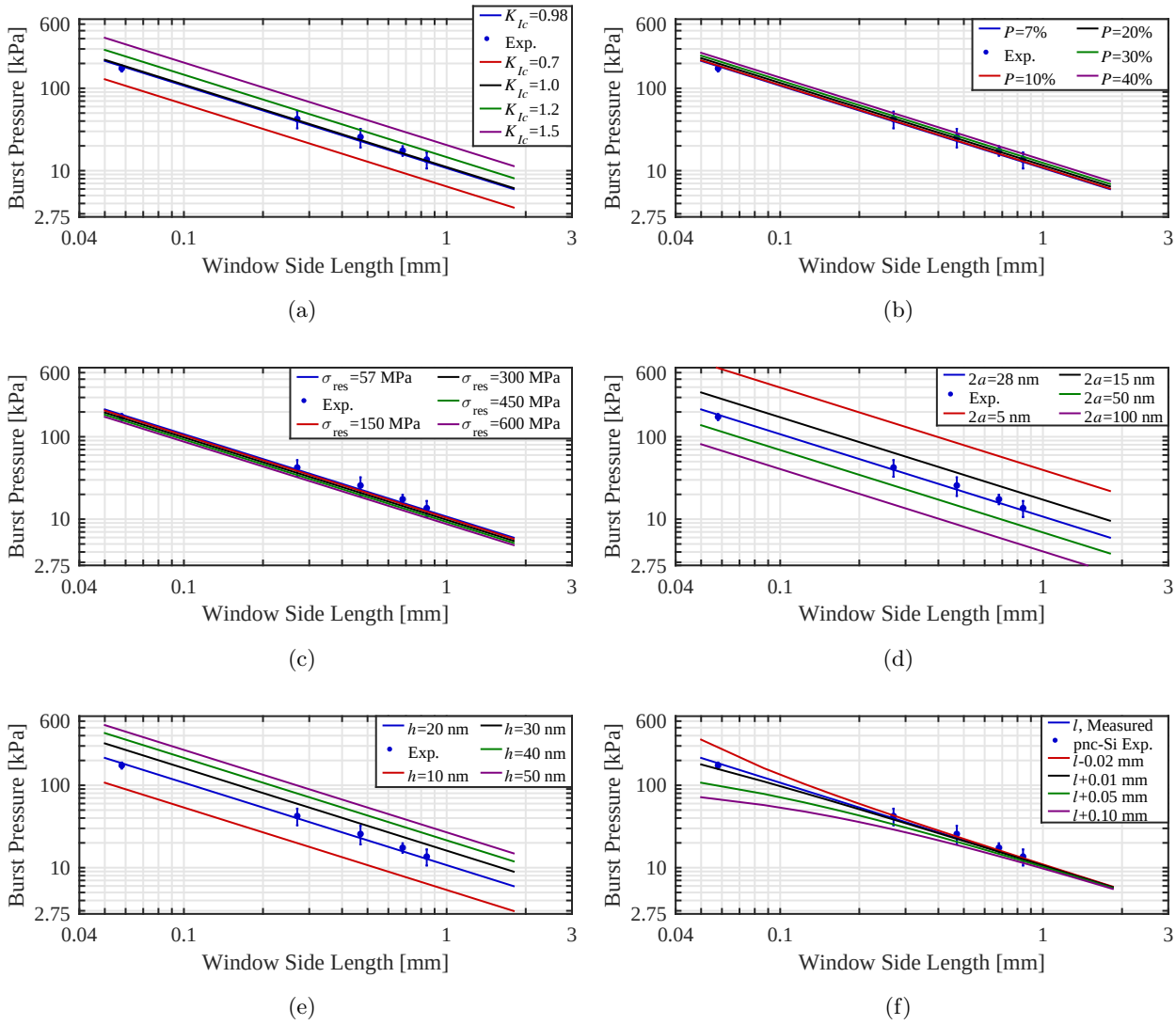


Figure 7: Exploring the parameter space using the numerical simulation. All blue lines are porous pnc-Si data from Figure 6 while additional trends represent changes in (a) fracture toughness, (b) porosity, (c) residual stress, (d) pore size, (e) membrane thickness, and (f) error in side length measurement. (Color online)

## 5 Discussion and Conclusions

We developed a mathematical model based on Griffith's law that predicts burst pressures of ultrathin porous membranes. Our experiments show that porous nanocrystalline silicon and silicon nitride membranes fail under catastrophic brittle fracture. Assuming a macroscopic brittle behavior and considering the size of the pores as the initial crack size, our model calculates the resultant bulge test pressure that membranes can withstand before fracture. The significant outcome of this

work is a mathematical model for predicting burst pressure that accounts for the effect of various structural parameters on the macroscopic behavior of the nanomembranes including variations in thickness, pore size, and porosity. The model predictions are in agreement with experimental results within 10% accuracy for square membrane dimensions from 60 μm to 1.5 mm. The model is very straightforward and only needs to fit to one parameter – fracture toughness. Unlike the previous approaches [17, 18], our new method does not require FEA for accuracy.

This publication deduces fracture toughness of porous NPN membranes to be much lower than their non-porous counterparts [2] in a bulge test scenario. Our mathematical model predicts a fracture toughness of $\sim 1.43$ MPa$\sqrt{\text{m}}$ for NPN membranes, while Merle and Göken [2] measured values around 6 MPa$\sqrt{\text{m}}$ for solid non-porous membranes. Although this discrepancy may appear problematic, we attribute the disagreement to experimental conditions. It should be noted that large variations in nanoscale fracture toughness values occur as a consequence of different loading conditions [24]. Merle and Göken fabricated defects in the center of their membranes which promoted failure in pure tension. In contrast, our membranes' defects lie at the boundaries which catalyzes failure under a combination of bending and tensile stress. The combination of bending and tension produces larger stresses compared to pure tension for the same applied bulge test pressure. To reinforce this significance, Matoy, *et al.* [20] have measured the fracture toughness for $SiN_x$ micro-cantilevers to be approximately 1.6 MPa$\sqrt{\text{m}}$ when subjected to pure bending. The findings of Matoy, *et al.* not only validate our observations, they lead to the conclusion that bending is most likely the dominant failure mode in NPN nanomembranes. Our observed fracture toughness of pnc-Si nanomembranes ($\sim 0.98$ MPa$\sqrt{\text{m}}$) is validated by its agreement to that of bulk monocrystalline silicon [25].

Another noteworthy conclusion from this work is increasing porosities enable the nanomembranes to withstand slightly higher pressure before failure (Figure 7b). Assuming that the size of the binding structures between pores (*i.e.* 'ligaments') is comparable to the size of the pores, this means that we see a strengthening effect by decreasing the ligament size. This strengthening behavior could arise from enhancements in the mechanisms governing ligament strength as their size decreases. For example, Zhou and Chen [26] reported a homogenous deformation in amorphous nanopillars with smaller layer thickness, while they observed localized

shear band formations in nanopillars with larger layer thicknesses. It is also possible that the ligaments at the nanoscale undergo some plasticity while the overall membrane behavior is brittle. Therefore more detailed investigations are needed to investigate the strengthening and fracture behavior of porous nanomembranes. Performing molecular dynamics simulations of a representative volume of pores and ligaments with various sizes will help to identify the mechanisms governing deformation and failure.

Nanomembranes are now used in research and commercial settings for separations [3, 9, 11], cell culture [4, 5], pumping [6], and sensing [7]. The volumes of fluids that can be processed in these applications are limited by the size of membranes that can be reliably constructed. Stronger membranes are not only less susceptible to bulge test failure, they result in higher yields during manufacturing and fewer failures during device assembly. Therefore, if a reliable understanding of the mechanics of nanomembrane failure can enable larger area devices, it can both lower cost and increase utility. The model developed here not only provides an excellent fit to the burst pressure data, it helps identify which parameters should be targeted in manufacturing in order to improve on nanomembrane mechanics.

Our work over the years has identified a nominal burst pressure value of $\sim$ 30 kPa correlates with success for routine use of membranes in most application areas. The experimental findings in this publication show that NPN crosses this threshold when membranes are smaller than $\sim$ 0.7 mm on a side while pnc-Si membranes require side lengths less than 0.25 mm to exceed this threshold. This finding is consistent with a significant increase in the number of devices and applications we have been able to explore since the introduction of NPN [13]. Since NPN and pnc-Si porosities, thicknesses, and elastic moduli are comparable, the primary explanation for the improved strength of NPN compared to pnc-Si appears to be the increase in fracture toughness. Ultimately we expect that atomistic simulations of nanomembranes will be the key to selecting materials and designing ultrastructures to maximize fracture toughness. More immediately, our sensitivity study identifies smaller pore sizes and increased membrane thickness as the parametric targets for improved membrane strength. Of course both of these parameters impact membrane performance as a molecular filter and thus any increases in strength must be weighed against performance goals.

# 6 Acknowledgments

The authors greatfully acknowledge valuable discussions with Dr. John Lambropoulos and Dr. Michael Skarlinski (Materials Science Program, University of Rochester) as well as with Dr. Karan Mehrotra (Corning Incorporated) during the development of this research. This work was funded by the National Science Foundation under award CBET:1159579.

## References

[1] J. Karch, R. Birringer, and H. Gleiter. Ceramics ductile at low temperature. *Nature*, 330:556–558, 1987.

[2] B. Merle and M. Göken. Fracture toughness of silicon nitride thin films of different thicknesses as measured by bulge tests. *Acta Materialia*, 59:1772–1779, 2011.

[3] Thomas R. Gaborski, Jessica L. Snyder, Christopher C. Striemer, David Z. Fang, Michael Hoffman, Philippe M. Fauchet, and James L. McGrath. High-performance separation of nanoparticles with ultrathin porous nanocrystalline silicon membranes. *ACS Nano*, 4(11):6973–6981, 2010.

[4] A.A. Agrawal, B.J. Nehilla, K.V. Reisig, T.R. Gaborski, D.Z. Fang, C.C. Striemer, P.M. Fauchet, and J.L. McGrath. Porous nanocrystalline silicon membranes as highly permeable and molecularly thin substrates for cell culture. *Biomaterials*, 31(20):5408–5417, 2010.

[5] Andrea R. Mazzocchi, Alan J. Man, Jon-Paul S. DesOrmeaux, and Thomas R. Gaborski. Porous membranes promote endothelial differentiation of adipose-derived stem cells and perivascular interactions. *Cellular and Molecular Bioengineering*, 7(3):369–378, 2014.

[6] Jessica L. Snyder, Jirachai Getpreecharsawas, David Z. Fang, Thomas R. Gaborski, Christopher C. Striemer, Philippe M. Fauchet, David A. Borkholder, and James L. McGrath. High-performance, low-voltage electroosmotic pumps with molecularly thin silicon nanomembranes. *Proceedings of the National Academy of Sciences of the United States of America*, 110(46):18425–18430, 2013.

[7] Maryna N. Kavalenka, Christopher C. Striemer, Jon-Paul S. DesOrmeaux, James L. McGrath, and Philippe M. Fauchet. Chemical capacitive sensing using ultrathin flexible nanoporous electrodes. *Sensors and Actuators B: Chemical*, 162(1):22–26, 2012.

[8] Hirohito Yamazaki, Shinji Kimura, Mutsumi Tsukahara, Keiko Esashika, and Toshiharu Saiki. Optical detection of DNA translocation through silicon nanopore by ultraviolet light. *Applied Physics A*, 115(1):53–56.

[9] Christopher C. Striemer, Thomas R. Gaborski, James L. McGrath, and Philippe M. Fauchet. Charge- and size-based separation of macromolecules using ultrathin silicon membranes. *Nature*, 445:749–753, 2007.

[10] Albert van den Berg and Matthias Wessling. Silicon for the perfect membrane. *Nature*, 445:726, 2007.

[11] Dean G. Johnson, Tejas S. Khire, Yekaterina L. Lyubarskaya, Karl J. P. Smith, Jon-Paul S. DesOrmeaux, Jeremy G. Taylor, Thomas R. Gaborski, Alexander A. Shestopalov, Christopher C. Striemer, and James L. McGrath. Ultrathin silicon membranes for wearable dialysis. *Advances in Chronic Kidney Disease*, 20(6):508–515, 2013.

[12] D.Z. Fang, C.C. Striemer, T.R. Gaborski, J.L. McGrath, and P.M. Fauchet. Methods for controlling the pore properties of ultra-thin nanocrystalline silicon membranes. *Journal of Physics: Condensed Matter*, 22(45), 2010.

[13] J.P.S. DesOrmeaux, J.D. Winans, S.E. Wayson, T.R. Gaborski, T.S. Khire, C.C. Striemer, and J.L. McGrath. Nanoporous silicon nitride membranes fabricated from porous nanocrystalline silicon templates. *Nanoscale*, 6:10798–10805, 2014.

[14] Stephen P. Timoshenko and S. Woinowsky-Krieger. *Theory of plates and shells*. McGraw-Hill Companies, 1959.

[15] J.J. Vlassak and W.D. Nix. A new bulge test technique for the determination of young's modulus and poisson's ratio of thin films. *Journal of Materials Research*, 7(12):3242–3249, 1992.

[16] Cees van Rijn, Michiel van der Wekken, Wietze Nijdam, and Miko Elwenspoek. Deflection and maximum load of microfiltration membrane sieves made with silicon micromachining. *IEEE Journal of Microelectromechanical systems*, 6(1):48–54, 1997.

[17] A. Kovács, Á. Kovács, M. Pogány, and U. Mescheder. Mechanical investigation of perforated and porous membranes for micro- and nanofilter applications. *Sensors and Actuators B: Chemical*, 127(1):120–125, 2007.

[18] Á. Kovács, A. Kovács, and U. Mescheder. Estimation of elasticity modulus and fracture strength of thin perforated sin membranes with finite element simulations. *Computational Materials Science*, 43:59–64, 2008.

[19] A.A. Griffith. The phenomena of rupture and flow in solids. *Philosophical Transactions of the Royal Society of London*, 221:163–198, 1921.

[20] Kurt Matoy, Helmut Schönherr, Thomas Detzel, Thomas Schöberl, Reinhard Pippan, Christian Motz, and Gerhard Dehm. A comparative micro-cantilever study of the mechanical behavior of silicon based passivation films. *Thin Solid Films*, 518:247–256, 2009.

[21] David Z. Fang. *Fabrication, Characterization, and Functionalization of Porous Nanocrystalline Silicon Membranes*. PhD thesis, University of Rochester, 2010.

[22] Marc Meyers and Krishan Chawla. *Mechanical Behavior of Materials: Second Edition*. Cambridge University Press, Ch. 7, pg. 427, 2009.

[23] J. Harrop and R.M. Abdul-Karim. Stresses and deflections in circular plates with square pitch perforations. *Nuclear Engineering and Design*, 6(5):431–439, 1967.

[24] Taechung Yi and Chang-Jin Kim. Measurement of mechanical properties for mems materials. *Measurement Science and Technology*, 10(8):706–706, 1999.

[25] G.R. Anstis, P. Chantikul, B.R. Lawn, and D.B. Marshall. A critical evaluation of indentation techniques for measuring fracture toughness: I, direct crack measurements. *Journal of the American Ceramic Society*, 64(9):533–538.

[26] Xiaoling Zhou and Changqing Chen. Strengthening and toughening mechanisms of amorphous/amorphous nanolaminates. *International Journal of Plasticity*, 80:75–85, 2016.